The Calculation of TTT and CCT diagrams for General Steels

N. Saunders[1], Z. Guo[2], X. Li[2], A.P. Miodownik[1] and J.-P. Schillé[2]

[1]Thermotech Ltd., Surrey Technology Centre, The Surrey Research Park
Guildford GU2 7YG, U.K.

[2]Sente Software Ltd., Surrey Technology Centre, The Surrey Research Park
Guildford GU2 7YG, U.K.

Abstract

Knowledge of the TTT or CCT diagrams of steels is an important factor in the thermo-mechanical processing of steels. Much experimental work has been undertaken to determine such diagrams. However, the combination of wide alloy specification ranges, coupled with sharp sensitivity to composition changes plus a dependency on grain size, means that it is impossible to produce enough diagrams for generalised use. To this end significant work has been undertaken over recent decades to develop models that can calculate TTT and CCT diagrams for steels. Almost without exception, these models have been shown to be limited in applicability to carbon and low alloy steels. The aim of the present work is to develop a model that can provide accurate TTT and CCT diagrams for general steels, including medium to high alloy types, tool steels, 13%Cr steels etc., for inclusion in the software programme JMatPro. This aim has been achieved and the present paper provides a background to the calculation method and present results of an extensive validation of the model against experiment.

Introduction

As part of the development of the software programme JMatPro, phase transformation models have been included for a variety of alloy types [1,2,3,4] e.g. Al-alloys, Ni-based superalloys, Ti-alloys and for TCP phases such as σ and χ in stainless steels. JMatPro also incorporated a capability to calculate transformations involving ferrite, pearlite and bainite in HSLA steels closely based on the model of Kirkaldy [2]. To bring this calculation capability in-line with JMatPro's capability for other alloys, where high alloy contents can be routinely handled, work has been undertaken to extend this model capability to steels of high alloy content.

There is a hugely extensive published literature concerned with the transformations in steels but, of this, only a small part is given over to the calculation of TTT and CCT diagrams. The pioneering work of Kirkaldy and co-workers [5,6] showed that it was possible to calculate quite accurate TTT and CCT diagrams as well as the Jominy hardenability for low alloy steels. Later work by Bhadeshia [7,8] used a different methodology to determine start curves for ferrite and bainite transformations and tested the model against experiment. The model of Bhadeshia has been extended by Lee [9,10] to cover slightly higher concentrations. However, although successful for low alloy steels these models are limited when it comes to more highly alloyed types.

One of the drawbacks of both models has been the use of dilute solution thermodynamics in calculating transformation temperatures. This can now be overcome using thermodynamic models [11] that provide high quality results for steels in general, ranging from stainless steels, to tool steels as well as the low to medium alloy range types.

The aim of the present work is to combine the more extensive thermodynamic models with a kinetic model to see if the composition range of applicability could be extended to cover a wider range of steels, including the highly alloyed types. The model of Kirkaldy was chosen as the basis for the new calculations as there is a clearly identifiable set of input parameters that are required and which can be readily calculated. It is also has empirical parameters that can be adjusted easily and controllably.

Transformation model

The model of Kirkaldy and co-workers

A model for the calculation of ferrite and pearlite was first presented by Kirkaldy et al. [5], following equations developed by Zener and Hillert [12,13]. In the initial model no attempt was made to differentiate between the diffusive and displacive transformations and a overall 'C' curve was produced using the general formula for the time (τ) to transform x fraction of austenite at a temperature T,

$$\tau(x,T) = \frac{1}{\alpha(N) D_{eff} \Delta T^{q}} \int_{0}^{x} \frac{dx}{x^{2(1-x)/3}(1-x)^{2x/3}} \tag{1}$$

where $\alpha=2\beta^{(N-1)/2}$, β is an empirical coefficient, N is the ASTM grain size, D is an effective diffusion coefficient, ΔT is the undercooling below the temperature where austenite is unstable with respect to ferrite (the Ae_3 temperature) and q is an exponent dependent on the effective diffusion mechanism.

They also assumed that the effective diffusion coefficient involving the alloying elements, analogous to a series resistance relationship (R_{eff}) such that

$$R_{eff} \propto \frac{1}{D_{eff}} \propto e^{\left(\frac{Q_{eff}}{RT}\right)} \sum_{j=1}^{m} \alpha_j C_j \tag{2}$$

where α_j is a constant for each element, j, C_j is the concentration of the element, j, and Q_{eff} is an effective activation energy for diffusion. The modified formula is given below

$$\tau_{TTT} = \frac{1}{2^{(N/8)}(\Delta T)^{3}} e^{\left(\frac{Q_{eff}}{RT}\right)} \sum_{j=1}^{m} \alpha_j C_j \tag{3}$$

The N term assumes an incubation transient whereby, for nucleation on grain surfaces, the time to a given volume transformed varies as the grain diameter to the ¼ power (hence the term $2^{N/8}$. The critical input parameters are then (1) the grain size, which should be known for each case, (2) the Ae_3 temperature which is calculated from thermodynamics, (3) the effective diffusion coefficient, Q_{eff}, and (4) the empirical constants α_j for each element. Q_{eff} and α_j were determined by empirically fitting curves derived using eq.3 to experimentally observed TTT curves and the final formula for calculating τ was given as

$$\tau_{0.1\%} = \frac{\exp\left(\frac{2000}{T}\right)}{2^{N/8}(Ae_3 - T)^3}(60.\%C + 90.\%Si + 160.\%Cr + 200.\%Mo) \tag{4}$$

where the amounts of each element are in wt%. The derivation as performed above means that, once the composition and grain size are provided, only the Ae_3 temperature needs to be calculated. The model was extended to include C-curves for pearlite and bainite and also to allow a general calculation for the amount of transformation as a function of time at temperature. This provided three sets of equations for the amount of transformation of ferrite (τ_F), pearlite (τ_P) and bainite (τ_B) [14].

$$\tau_F = \frac{60.\%Mn + 2.\%Ni + 68.\%Cr + 244.\%Mo}{6 \times 2^{N/8} \Delta T^3 D_F} I \tag{5}$$

$$\tau_P = \frac{1.8 + 5.4(\%Cr + \%Mo + 4.\%Mo.\%Ni)}{6 \times 2^{N/8} \Delta T^q D_P} I \tag{6}$$

and

$$\tau_B = \frac{(2.3 + 10.\%C + 4.\%Cr + 19.\%Mo).10^{-4}}{6 \times 2^{N/8} \Delta T^2 \exp(-27,500/RT)} I \tag{7}$$

where ΔT is the undercooling below the relevant transformation temperature of ferrite, pearlite and bainite. D_F and D_P are given by equations 8 and 9 below.

$$D_F = \exp(-23,500/RT) \tag{8}$$

$$\frac{1}{D_P} = \frac{1}{\exp(-27,500/RT)} + \frac{0.5Mo}{\exp(-37,000/RT)} \tag{9}$$

The parameter I to the right of equations 5-7 is the volume fraction integral as shown on the right of equation 1. For bainite the integral is partially corrected to account for experimental observation [14].

Once the TTT diagram is calculated, it is possible to transform it into a CCT diagram using well-established additivity rules after Kirkaldy [5,6,14].

Current modifications to Kirkaldy's model

For the calculation of τ_B equation 7 is used as shown. However, a reassessment of the empirical formula to calculate the bainite start temperature (T_{Bs}) has been undertaken. For τ_F

and τ_P the basic structure of the equations has been taken as above, with the volume fraction integral retained as is the grain size dependency of the rate of transformation. However, following Lee and Bhadeshia [9] we have made q composition dependent, becoming slightly lower than 3 with increasing levels of Cr, Mo and W, and we have more generally made D_F and D_P composition dependent. For the case of the linear composition dependencies these have been modified and mainly used to account for interactions between solutes, i.e. Cr and Mo.

For the case of ferrite, it was found that the observed behaviour could be best accounted for with a sigmoidal type of relationship for the activation energy for diffusion. This remains close to that given by equation 8 at low alloying levels for low alloy steels but changes quite sharply with the addition of certain elements, such as Cr, Mo and W before levelling off to a constant value at high concentrations. The adjustment of the diffusion coefficient is taken to indicate, following Kirkaldy [14], that solute drag effects are becoming important with these elements. We have also found that strong interactions between certain solutes were required to account for sluggish transformations. This was particularly true for Ni-Cr-Mo steels and may indicate particular solute effects with respect to the diffusion coefficient. But it may equally well relate to a thermodynamic effect associated with a greater stability of austenite in the Fe-Ni-Cr-C system than is accounted for with the current thermodynamic calculations.

Martensite calculations

The most commonly used formula for calculating the martensite start temperature (M_S) is drawn from Andrews [15], which provides a good benchmark for low to medium alloy steels. Unfortunately, the accuracy of Andrew's formula falls away drastically at higher alloy contents. Recent work by Ghosh and Olson [16] has attempted to extend the compositional limits to high alloy steels by using an approach linked to the T_0 temperature between undercooled austenite and ferrite. This is successful when $M_S > 100$ºC, but there are problems when this approach is extended to alloys with low or sub-zero values for M_S and Co needs to be treated as a special case.

While a T_0 approach is theoretically favoured, it is likely that many of the problems encountered by Ghosh and Olson [16] can be attributed to the need to incorporate a more sophisticated magnetic model for iron, which explicitly recognises the 2 gamma state electronic contribution. There are current moves to recognise this need [17], but the complex magnetic behaviour that arises through alloying [18] makes its inclusion in a multi-component thermodynamic database is unlikely in the near future. Therefore an essentially empirical approach to incorporating some features of the two gamma state model has been used. In addition, unlike most previous attempts the present approach incorporates certain important features of a full thermodynamic treatment, notably that each element makes a contribution to the stability of both the parent and the product phases and therefore is not treated rigidly as an austenite or ferrite (martensite) stabiliser. By combining suitable mathematical functions, the model automatically generates different behaviour of elements in different concentration ranges and in different solute environments.

The importance of determining the correct austenite composition is also an important feature of the current integrated treatment if carbides or other second phases are present, or if the alloy is quenched from the austenite/ferrite two-phase region, it is inappropriate to use the overall alloy composition. In the present treatment, the composition of austenite at the quench temperature is always calculated directly and used in the required model equations.

The M_S model has been further extended to calculate the amount of martensite as a function of undercooling below the M_S. As with the determination of the M_S itself, previous suggested formulae have not generally been able to handle large composition ranges, whereas the current model has achieved this by relating the volume fraction of martensite to the temperature dependence of the entropy of transformation.

Results and Discussion

For the validation of the model we have used two sources of experimentally determined TTT diagrams. (i) The Atlas of Isothermal Transformation Diagrams of BS En Steels [19] and (ii) the ASM Atlas of Isothermal Transformation and Cooling Transformation Diagrams [20].

For the En steels the austenisation temperature and grain size is provided in all cases. For the latter we have used the reported as-quenched grain size. This atlas is particularly useful as for a good number of steels the effect of C is specifically tested, as is the effect of changing the austenisation temperature. As noted for the martensite calculations, the actual composition of austenite at the quench temperature is used.

As it is necessary to have both the austenitising temperature and grain size data, the steels drawn from the ASM atlas have been confined largely to low and medium alloy steels. This means that, in the main, USS steel diagrams were used. For the case of tool steels grain sizes are not generally reported. However it is considered important that the model should be tested for such highly alloyed steels. To this end we have made the following assumptions. For high speed steels, where the carbide is formed during solidification, a grain size of 10μm was used, after Elliott [21], and for other tool steels an ASTM grain size of 8 was used. This does involve an inherent inaccuracy, but allows a reasonable test to be made for such steels.

We have calculated TTT diagrams for more than 100 steels and compared these with experiment. Direct comparisons are shown for four alloys. (i) For low alloy steel 5140 (Fig.1), (ii) for a medium alloyed NiCr steel En 36 (Fig.2) (iii) for a T1 high speed steel (Fig.3) and (iv) for a En 56, 13%Cr rust-resistant steel (Fig.4). Calculated M_S, M_{50} and M_{90} temperatures are also shown in the figures.

While Figures 1-4 provide detail for specific calculations, it is instructive to look at overall accuracy of the calculations. To this end we have taken the experimentally observed start times at the nose temperature of the various transformations to ferrite, pearlite and bainite and compared these to those calculated using the new model. In this way it is possible to gain a good measure of the overall accuracy. In some cases, particularly for fast transformation steels, it was not possible to clearly differentiate nose temperatures for the various transformations. For example, the ferrite, bainite and pearlite transformations appear merged into a continuous C-curve in the experimental work. The calculated transformation of the fastest phase was taken in such circumstances

Figure 5 shows the comparison, breaking the results down between the En steels and the ASM atlas steels. We have avoided “double counting” where the same steels are shown both in the En steel atlas and the ASM atlas. In particular, the En steel atlas has extensive coverage for NiCr and NiCrMo steels. For these steels comparison is made only to the

En steel atlas. In both plots the dashed lines representing an error of 3× and have been included for guidance.

The comparison between calculation and experiment is very good and represents a substantial advance over previous models whose range of validity centred largely on C and low alloy steels. It is further instructive to analyse the results in terms of statistical accuracy and Table 1 shows the percentage of results lying in various accuracy bands. It can be seen that between 80% of calculated results are within a factor of 3 of experiment while almost 90% lie within a factor of 4. To emphasise the high levels of alloying that have been used in the comparison studies, Table 2 shows the maximum levels of particular elements added as well as the lowest level of Fe in any one alloy.

The method to convert a TTT diagram into a CCT diagram is well established and has been tested in earlier papers [5,6,14], so no further discussion will be presented here, except this capability has been included in JMatPro.

We have also tested the martensite temperature calculations for M_S, M_{50} and M_{90}. The main source for experimental comparison has been the BSC atlas of continuous cooling diagrams [22], where results for all three values are reported for a wide range of steels. As can be seen, the predictions have a high accuracy.

Summary and conclusions

Work has been undertaken to develop a model for the calculation of TTT and CCT diagrams for generalised steels. The work has achieved a high degree of success and has been extensively validated against wide ranging types of steel.

References

1. N. Saunders, Z. Guo, X. Li, A.P. Miodownik and J-Ph. Schillé, *JOM*, 55(12) (2003), 60.
2. N. Saunders, X. Li, A.P. Miodownik and J-Ph. Schillé, *Materials Design Approaches and Experiences*, eds. J.-C. Zhao et al., (Warrendale, PA:TMS, 2001), 185.
3. N. Saunders, to be published in *Proc. 9th International Conference on Aluminium Alloys*, 2-5 August, Brisbane, Australia, 2004.
4. N. Saunders, X. Li. A.P. Miodownik and J.-Ph. Schille, to be published in *Ti-2003 Science and Technology*, ed. G. Luetering, (Weinheim, Germany: Wiley-VCH, 2004)
5. J.S. Kirkaldy, B.A. Thomson, and E.A. Baganis, *Hardenability Concepts with Applications to Steel*, eds. J.S. Kirkaldy and D.V. Doane, (Warrendale, PA: AIME, 1978), 82.
6. J.S. Kirkaldy and D.Venugopolan, *Phase Transformations in Ferrous Alloys*, eds. A.R. Marder and J.I. Goldstein, AIME, (Warrendale, PA: AIME, 1984), 125.
7. H.K.D.H. Bhadeshia, Met. Sci., 15 (1981), 175.
8. H.K.D.H. Bhadeshia, Met. Sci., 16 (1982), 159.
9. J.-L. Lee and H.K.D.H. Bhadeshia, *China Steel Technical Report,* No.6 (1992), 19.
10. J.-L. Lee and H.K.D.H. Bhadeshia, *Mater. Sci. Eng.*, A171 (1993), 223.
11. N. Saunders and A.P. Miodownik, *CALPHAD – Calculation of Phase Diagrams, Pergamon Materials Series vol.1*, ed. R.W. Cahn (Oxford: Elsevier Science,1998).
12. C. Zener, *Trans.AIME*, 167 (1946), 550.

13. M. Hillert, *Jerkontorets Ann.*, 141 (1957), 758.
14. J.S. Kirkaldy, *Scand. J. Met.*, 20 (1991), 50.
15. K.W. Andrews, *J. Iron & Steel. Inst.*, 183 (1965), 721.
16. G. Ghosh and G.B. Olson, *J. Phase Equilibria*, 22 (2001), 199.
17. Q. Chen and B. Sundman, *J. Phase Equilibria*, 22 (2001), 631.
18. D. de Fontaine, S.G. Fries, G. Inden, A.P. Miodownik, R. Schmid-Fetzer and S.L. Chen, *CALPHAD*, 19 (1995), 499.
19. *Atlas of Isothermal Transformation Diagrams of BS En Steels*, Special report No.56 (London: The Iron and Steel Institute, 1956)
20. *Atlas of Isothermal Transformation and Cooling Transformation Diagrams*, (Metals Park, OH: 1977).
21. G. Hoyle, *High Speed Steels*, (London : Butterworths, 1988), 114.
22. M. Atkins, *Atlas of Continuous Cooling Transformation Diagrams for Engineering Steels,* (Sheffield: British Steel Corporation, 1977).

Table 1. Percentage of calculated results within specified accuracy limit

Accuracy factor	×2	×3	×4	×5
Percentage of results within accuracy factor	70%	80%	88%	92%

Table 2. Maximum level of alloying addition in steels used for validation of model. Also shown is the minimum level of Fe.

	max/min level
Fe	> 75
C	< 2.3
Si	< 3.8
Mn	< 1.9
Ni	< 8.9
Cr	< 13.3
Mo	< 4.7
V	< 2.1
W	< 18.6
Al	< 1.3
Cu	< 1.5
Co	< 5.0

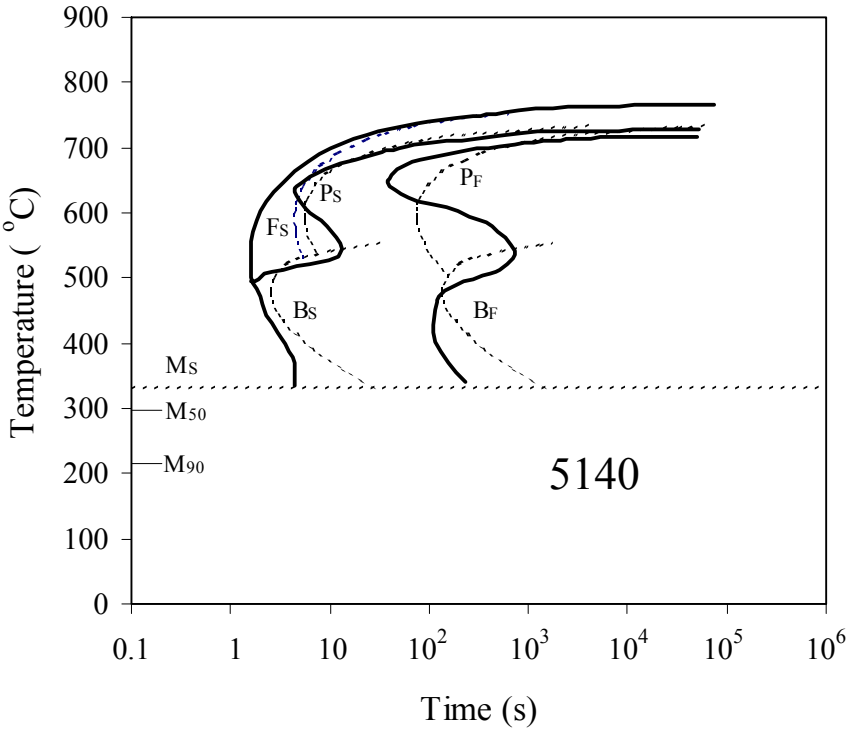

Figure 1. Comparison between experimental [17] and calculated TTT diagram for a 5140 steel, composition Fe-0.42C-0.68Mn-0.16Si-0.93Cr (wt%)

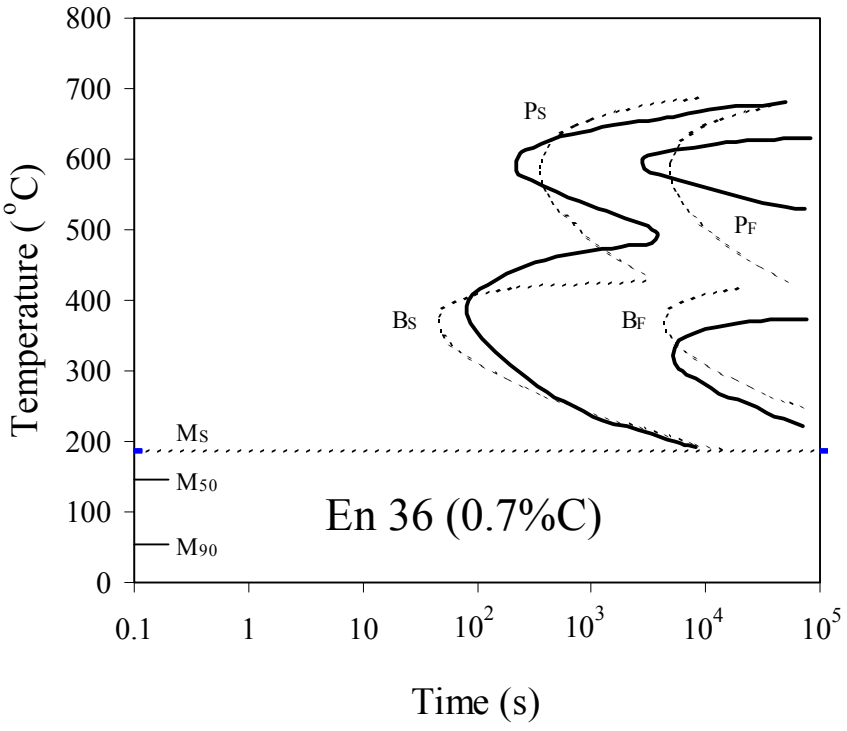

Figure 2. Comparison between experimental [16] and calculated TTT diagram for a En36 carburised steel, composition Fe-0.7C-0.35Mn-0.16Si-3.24Ni-0.96Cr-0.06Mo (wt%)

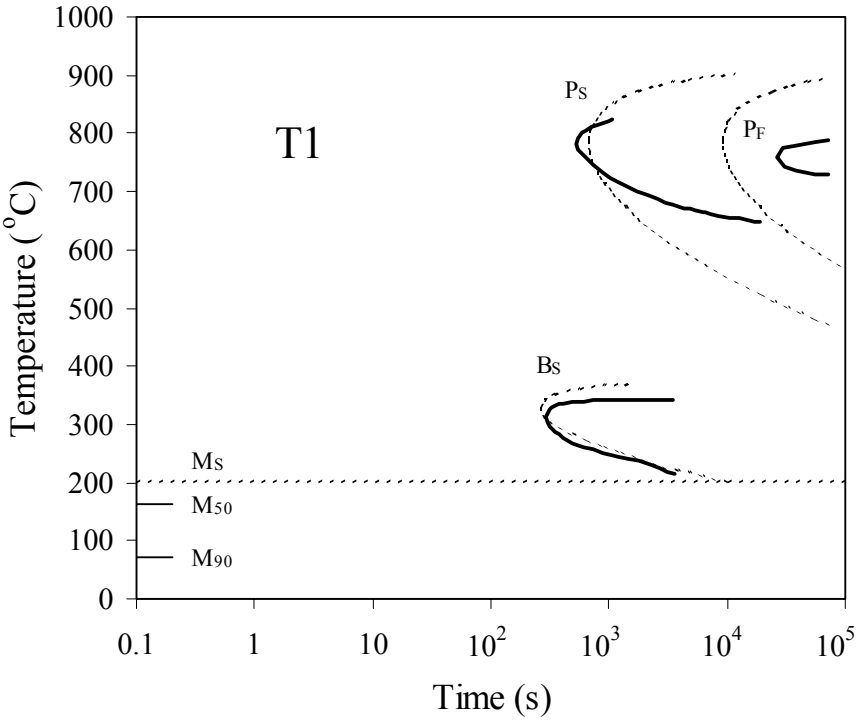

Figure 3. Comparison between experimental [16] and calculated TTT diagram for T1 high speed steel, composition Fe-0.72C-0.27Mn-0.39Si-4.09Cr-1.25V-18.59W (wt%)

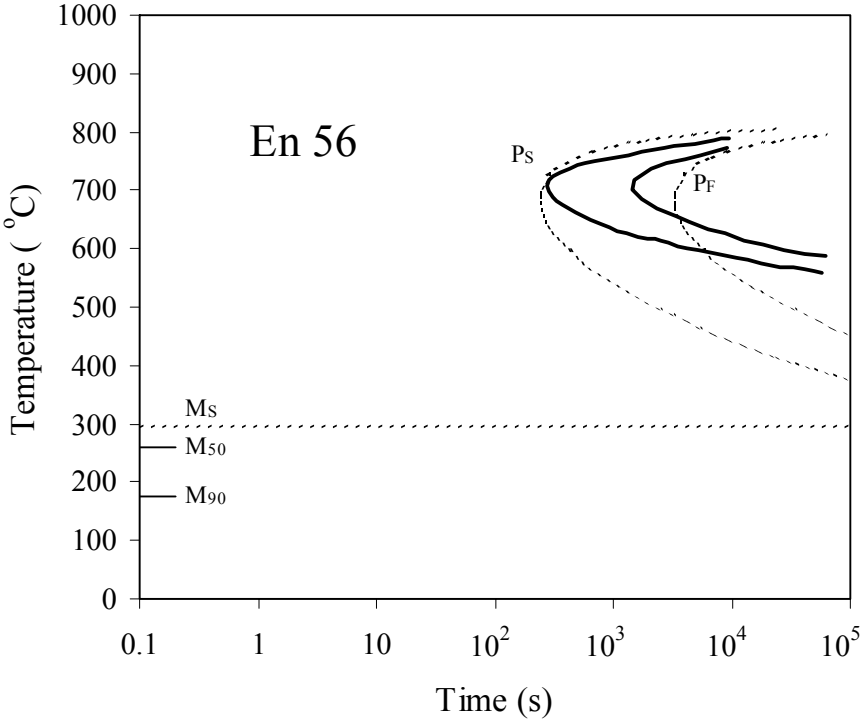

Figure 4. Comparison between experimental [16] and calculated TTT diagram for En56 Cr rust-resisting steel, composition Fe-0.24C-0.27Mn-0.37Si-0.32Ni-13.3Cr-0.06Mo (wt%)

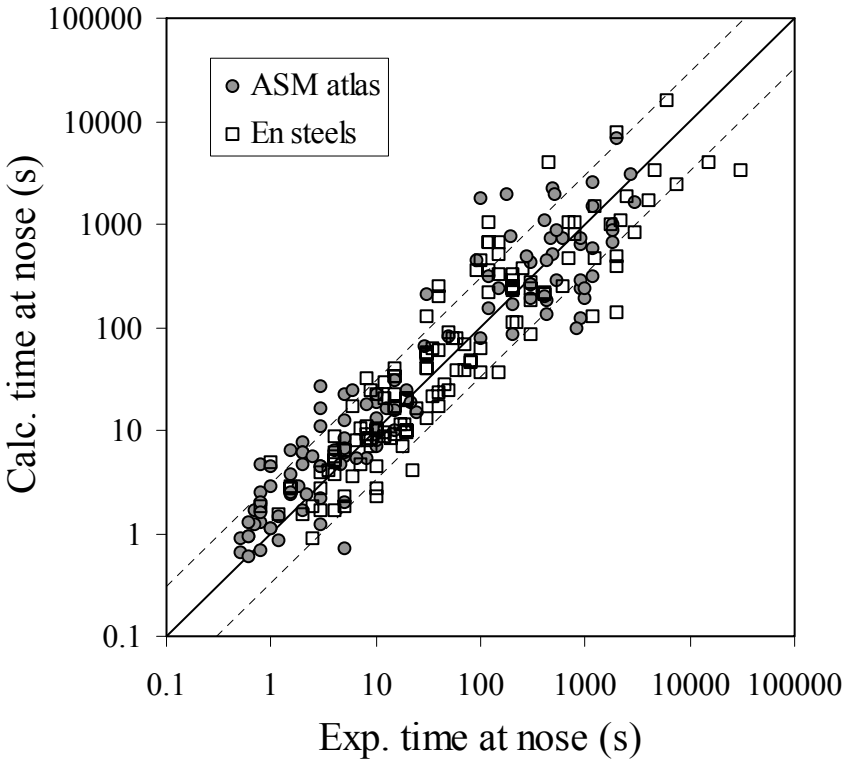

Figure 4. Comparison between experimental and calculated start times at the nose temperature of the C-curves for various steels.

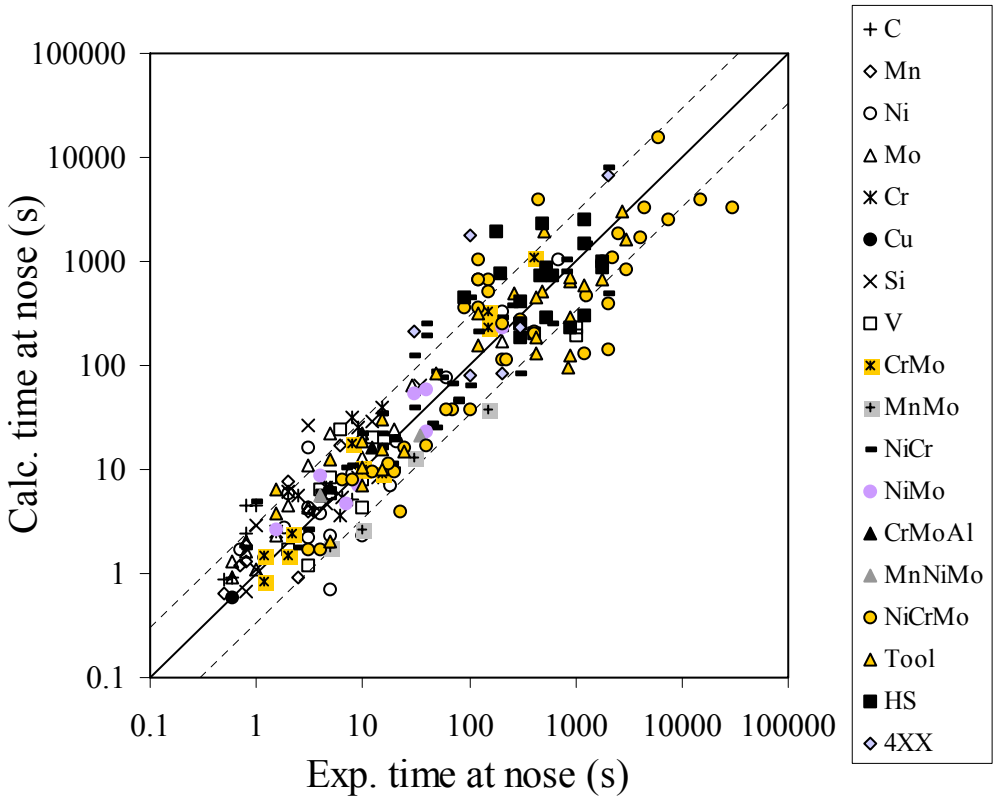

Figure 5. Comparison between experimental and calculated start times at the nose temperature of the C-curves for various steels showing results by steel type.

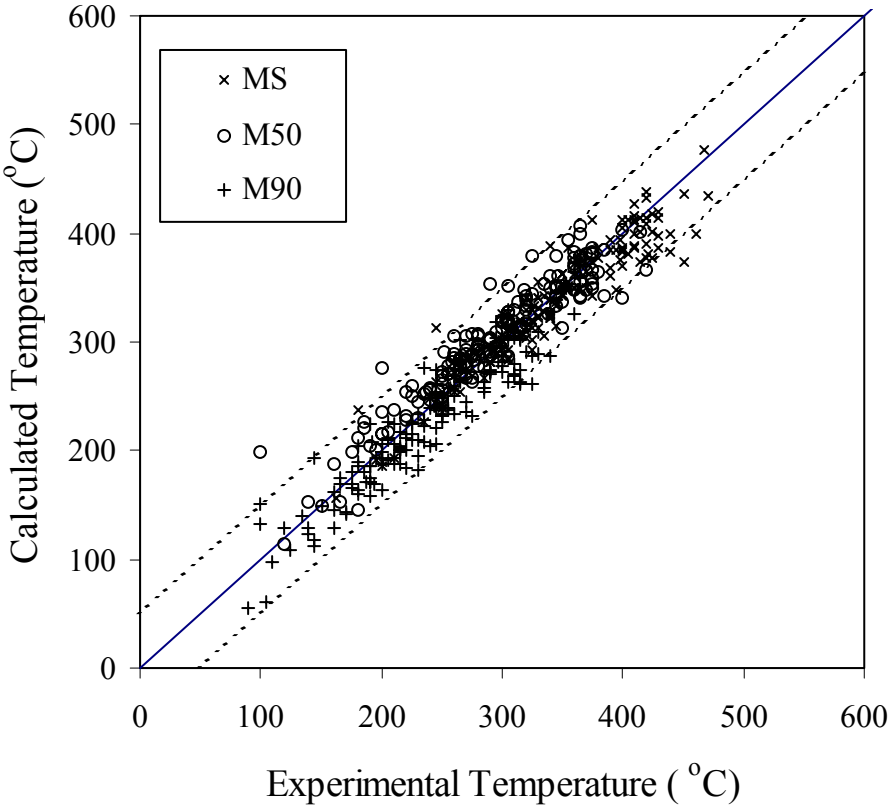

Figure 5. Comparison between experimental and calculated martensite temperatures for various steels.